Infrared Physics & Technology 85 (2017) 74–80

Contents lists available at ScienceDirect

Infrared Physics & Technology

journal homepage: www.elsevier.com/locate/infrared

Regular article

Noise characteristics analysis of short wave infrared InGaAs focal plane arrays

Chunlei Yu [a,b,c], Xue Li [a,b], Bo Yang [a,b,d], Songlei Huang [a,b], Xiumei Shao [a,b], Yaguang Zhang [a,b,c], Haimei Gong [a,b,*]

[a] State Key Laboratories of Transducer Technology, Shanghai Institute of Technical Physics, Chinese Academy of Sciences, Shanghai 200083, China
[b] Key Laboratory of Infrared Imaging Materials and Detectors, Shanghai Institute of Technical Physics, Chinese Academy of Sciences, Shanghai 200083, China
[c] University of Chinese Academy of Sciences, Beijing 100049, China
[d] State Key Laboratories of Functional Materials for Informatics, Shanghai Institute of Microsystem and Information Technology, Shanghai 200050, China

HIGHLIGHTS

- This paper presents the theoretical analysis of FPA noise, and point out that both dark current and detector capacitance strongly affect the FPA noise.
- Several InGaAs FPAs were measured and analyzed, the experiments' results could be well fitted to the calculated results.
- The study found that the major contributor of FPA noise is coupled noise with shorter integration time. The influence of detector capacitance on FPA noise is more significant than that of dark current.
- To investigate the effect of detector performance on FPA noise, two kinds of photodiodes with different concentration of the absorption layer were fabricated. The detectors' performance and noise characteristics were measured and analyzed, the results are consistent with that of theoretical analysis.

ARTICLE INFO

Article history:
Received 21 March 2017
Revised 24 May 2017
Accepted 25 May 2017
Available online 27 May 2017

Keywords:
InGaAs
FPAs
Noise characteristics
Capacitance of detectors

ABSTRACT

The increasing application of InGaAs short wave infrared (SWIR) focal plane arrays (FPAs) in low light level imaging requires ultra-low noise FPAs. This paper presents the theoretical analysis of FPA noise, and point out that both dark current and detector capacitance strongly affect the FPA noise. The impact of dark current and detector capacitance on FPA noise is compared in different situations. In order to obtain low noise performance FPAs, the demand for reducing detector capacitance is higher especially when pixel pitch is smaller, integration time is shorter, and integration capacitance is larger. Several InGaAs FPAs were measured and analyzed, the experiments' results could be well fitted to the calculated results. The study found that the major contributor of FPA noise is coupled noise with shorter integration time. The influence of detector capacitance on FPA noise is more significant than that of dark current. To investigate the effect of detector performance on FPA noise, two kinds of photodiodes with different concentration of the absorption layer were fabricated. The detectors' performance and noise characteristics were measured and analyzed, the results are consistent with that of theoretical analysis.

1. Introduction

InGaAs-based FPAs for SWIR imaging have extensive application and development prospects in space remote sensing [1–4]. The spectral response of $In_{0.53}Ga_{0.47}As$ p-i-n photodiodes typically covers 0.9–1.7 μm at room temperature. In this band, the detectors can be applied to the foggy and smoky environment [5–7]. InGaAs FPAs consist of InGaAs detector arrays and the silicon readout integrated circuit (ROIC). The technology is evolving to smaller pixel pitch, larger formats, lower noise, higher operating temperature and lower production cost [8]. To enable very low light imaging capabilities and improve the signal to noise ratio, sensor noise levels must be reduced, which requires extremely low dark current and the readout noise of ROIC. This demands careful InGaAs material growth, detector processing and ROIC design [9].

Sometimes shot noise from dark current is the major contributor to FPA noise. However, in applications like Adaptive Optics, the contribution of dark current to the total noise is insignificant at a high frame rate. In this case, the readout noise of the ROIC would

* Corresponding author at: State Key Laboratories of Transducer Technology, Shanghai Institute of Technical Physics, Chinese Academy of Sciences, Shanghai 200083, China.
E-mail address: hmgong@mail.sitp.ac.cn (H. Gong).

http://dx.doi.org/10.1016/j.infrared.2017.05.017
1350-4495/

be dominant in FPA noise [10]. Furthermore, there have been improvements in reducing the detector dark current density, which can be reduced to 0.7 nA/cm^2 at 290 K [11]. Thus, the contribution of ROIC noise is more significant. In previous studies, the ROIC noise was considered to be associated with the design of ROIC only. However, by our study found that the detector capacitance could be one of the critical influences on ROIC noise. From the detector performance perspective, both dark current and detector capacitance greatly affect FPAs noise. This paper presents a mathematical analysis of FPAs noise. The FPAs noise characteristic and detector arrays performance was studied systematically by fabrication and measurement of several InGaAs FPAs and photodiodes.

2. Noise analysis of FPA

It is necessary to analyze the noise mechanisms carefully to obtain low-noise performance FPAs [12]. The InGaAs FPA noise mainly includes shot noise, detector thermal noise, detector 1/f noise, CTIA KTC noise, 1/f noise, amplifier thermal noise, KTC noise from sample circuit, fixed pattern noise and so on [13].

The shot noise $\bar{V}^2_{shot}$ and detector thermal noise $\bar{V}^2_{dth}$ can be given by:

$$\bar{V}^2_{shot} = \frac{qI_{dc}}{C^2_{int}}\tau_{int}, \tag{1}$$

$$\bar{V}^2_{dth} = \frac{2k_BT}{R_dC^2_{int}}\tau_{int}, \tag{2}$$

where I_{dc} is dark current, C_{int} is integration capacitance, τ_{int} is integration time, R_d is photodiode resistance. Usually R_d is so high that the detector thermal noise could be neglected.

The CTIA KTC noise and low-frequency 1/f noise can be effectively restrained by correlated double sampling (CDS), while the sampling circuit will cause both the KTC noise and the amplifier thermal noise to increase because of double samples [14]. The KTC noise from sample circuit and the amplifier thermal noise can be represented by [15]:

$$\bar{V}^2_{sample} = \frac{2k_BT}{C_s}, \tag{3}$$

$$\bar{V}^2_{ath} = \frac{4\alpha k_B\mathrm{T}(C_{int}+C_d)^2}{C_{int}(C_LC_{int}+C_LC_d+C_dC_{int})}, \tag{4}$$

while C_s is sampling capacitance, C_L is load capacitance, C_d is detector capacitance, α called excess noise factor is used to describe the contribution to noise of active load, with a typical value of 1–2.

The amplifier thermal noise is a part of ROIC noise but related to the detector capacitance. It is called coupled noise, because this noise is generated from the coupling of photodiode and the input stage circuit in ROIC. Therefore, it is significant to decrease the detectors capacitance to fully realize the low noise ROIC as designed.

The fixed pattern noise originates from performance differences of each pixel caused by the ROIC materials and manufacturing process. This noise is proportional to τ^2_{int}. There is another kind of noise called detector 1/f noise which is also proportional to τ^2_{int}. The flicker noise is caused by various impurities and defects of semiconductor internal or the surface.

The value of FPAs total noise could be represented by quadratic function of integration time (τ_{int}):

$$\bar{V}^2_{total} = A + B\times\tau_{int} + C\times\tau^2_{int}, \tag{5}$$

The constant term is readout noise, mainly coupled noise. The linear noise is detectors noise, mainly shot noise. The quadratic term is fixed pattern noise. Therefore, the different components of noise can be quantified by polynomial fitting $V^2_{total}-\tau_{int}$ curves. The main source of FPA noise can be analyzed by linear fitting $\log V_{total}-\log\tau_{int}$ curves [16]. The fitting slope is indicative of the major contributor in total noise: 0, 0.5 and 1 indicate that the coupled noise, shot noise, and fixed pattern noise are the main sources respectively. Between these adjoining points the effect is imposed by combination of the two corresponding kinds of noise.

The coupled noise and shot noise are closely related to detector capacitance and dark current respectively. As shown in Fig. 1, the effect of detector capacitance on FPAs noise in various situations can be visualized by comparing it to the dark current. The lines mean the watershed where the contribution of detector capacitance to FPAs noise is equal to dark current. On the left side of them, the coupled noise excesses the shot noise. While on the right side, the shot noise from dark current is more crucial.

As shown in Fig. 1(a), the smaller the pixel pitch becomes, the less the corresponding slope is, which means the role that the detector capacitance plays on total noise gradually becomes more important. For example, at a detector capacitance level of 100 fF and a pixel pitch of 30 μm, the coupled noise is not dominant until the dark current density decreases to 1 nA/cm^2. However, for 10 μm pixels, the same capacitance of 100 pF becomes the major contributor of noise as long as dark current density is below 18 nA/cm^2. Therefore, it's very important to reduce the detector capacitance further as the pitch decreases in size while maintaining a low dark current density.

As shown in Fig. 1(b) shows that as the integration time rises, the contribution of dark current of the dark current to FPAs noise increases. At a detector capacitance level of 100 fF and integration time of 50 ms, the shot noise dominates FPAs noise if dark current density is above 8 nA/cm^2. For integration time of 500 ms, at the same capacitance of 100 pF, shot noise is significant when dark current density is greater than 1 nA/cm^2.

As shown in Fig. 1(c), the higher integration capacitance makes the total noise more dependent on the dark current. At a detector capacitance level of 100 fF and integration capacitance of 30 fF, coupled noise is not dominant until the dark current decreases to 0.5 nA/cm^2. For integration capacitance of 150 fF, the same capacitance of 100 pF, the coupled noise is remarkable when dark current is below 13.6 nA/cm^2.

Given that the smaller size, shorter integration time and larger integration capacitance are pursed, it's of great importance to extremely reduce the detector capacitance, while maintaining a low dark current density.

3. Experimental details

Noise characteristics of InGaAs FPAs were measured by the FPA noise measurement system as shown in Fig. 2. The response voltage of every pixel in InGaAs FPAs was sampled continuously by FPAs measurement system, and then the response voltage and noise voltage were calculated using a statistical approach. Therefore, the total noise V_{total} of FPAs could be obtained as a function of integration time τ_{int}. I-V and C-V characteristics of photodiodes at different temperature were measured by semiconductor parameter analyzer (Agilent Technologies B1500A).

Two InGaAs FPAs operated in the 1.0–1.7 μm spectral range, marked by S1 and S2, were measured at room temperature. The FPAs consist of InGaAs photodiodes and Si ROIC with capacitor feedback trans-impedance amplifier (CTIA) input stage circuit and correlated double sampling (CDS) structure. The photodiodes were fabricated by n-i-n epitaxial materials, planar diffusion

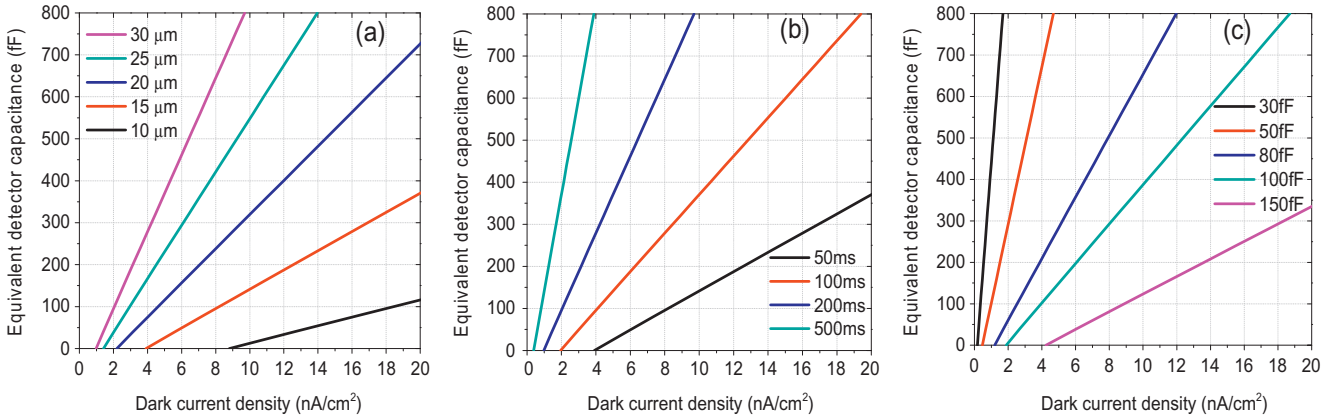

Fig. 1. Effect of detector capacitance versus dark current density. The lines represent where the coupled noise is equal to shot noise. (a) For different pixel pitches. (b) For different integration time. (c) For different integration capacitance.

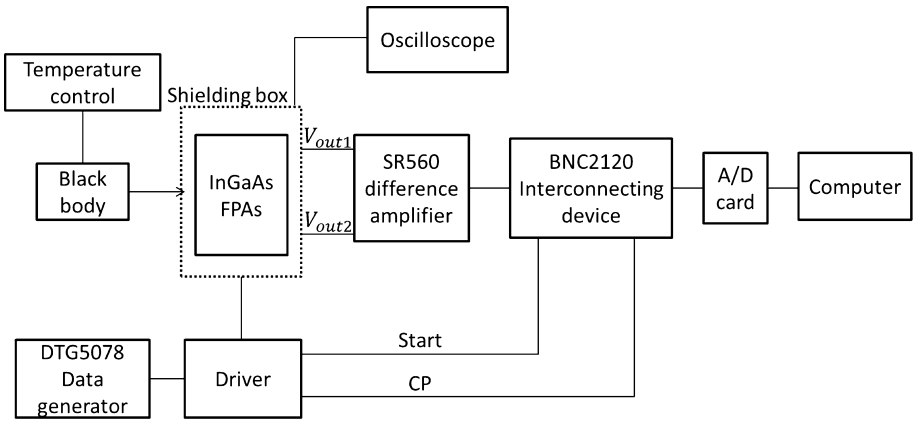

Fig. 2. The schematic of noise measurement system.

process and a surface passivation silicon nitride coating film. The concentrations of two samples' InGaAs absorption layers may not be equal ($N_{S1} = 5 \times 10^{16}$ cm^{-3}, N_{S2} is not demarcated). The parameters of involved InGaAs FPAs are shown in Table 1.

In order to further analyze the influences of detector performances on FPAs noise, InGaAs photodiodes marked by P1 and P2 with different concentrations of absorption layers were fabricated by the same processing as S1. The photodiode epitaxial structure and the schematic of the pixel unit cell are shown in Fig. 3. The parameters of the involved InGaAs photodiodes are shown in Table 2.

4. Results and discussion

The noise characteristics of different InGaAs FPAs at room temperature were studied by analyzing the relationship between noise and integration time. The $V_{total}^2 - \tau_{int}$ curve of S1 at room temperature and its polynomial fitting curve are shown in Fig. 4.

The polynomial fitting result is,

$$V_{total}^2 = 5.60 \times 10^{-7} + 4.29 \times 10^{-6} \times \tau_{int} + 3.41 \times 10^{-6} \times \tau_{int}^2, \quad (6)$$

According to the mathematical analysis of FPAs noise above, the constant term is readout noise, which depends on not only the ROIC but also the detector capacitance. The linear term is detector noise from the dark current. I-V and C-V characteristics of S1 at room temperature were shown as Fig. 5. The dark current of S1 is 3.96×10^{-14} A at room temperature and 100 mV reverse bias, and the detector capacitance is 670 fF at 0 V.

The constant and linear terms can be calculated by using the measured values and parameters in Table 1.

$$A = V_{sample}^2 + V_{coupled}^2 = 1.63 \times 10^{-7} + 3.94 \times 10^{-7} = 5.57 \times 10^{-7}, \quad (7)$$

$$\begin{aligned} B \cdot \tau_{int} &= V_{shot}^2 + V_{thermal}^2 \\ &= 1.32 \times 10^{-6} \times \tau_{int} + 2.32 \times 10^{-6} \times \tau_{int} = 3.64 \times 10^{-6} \times \tau_{int}, \end{aligned} \quad (8)$$

Fig. 6 shows the comparison of measured and fitted results. It is obvious that the measured constant term fits the fitted one well. However, the measured linear term increasingly undershoots the fitted with integration time going up. The linear noise does not

Table 1
The parameters of InGaAs FPAs.

Sample name	Concentration of absorption layer (cm^{-3})	Active area (μm^2)	C_{int} (fF)	C_s (fF)	C_L (fF)
S1	5×10^{16}	30×30	72	50	300
S2	Not demarcated	30×30	72	50	300

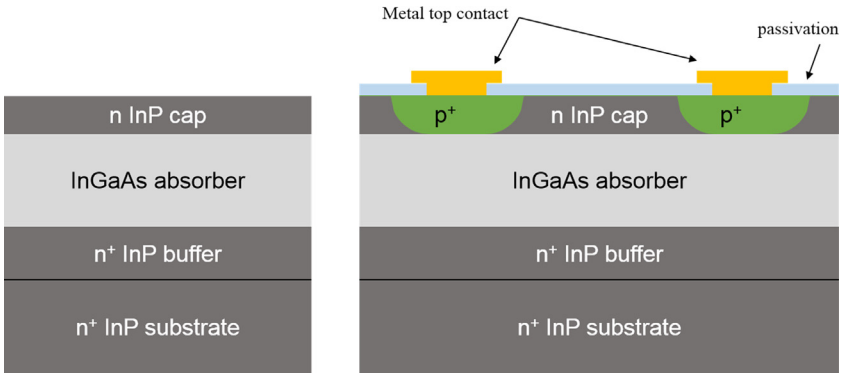

Fig. 3. (a) The photodiode epitaxial structure (b) the schematic of the pixel unit cell.

Table 2
The parameters of InGaAs photodiodes.

Sample name	Concentration of absorption layer (cm^{-3})	Active area (μm^2)
P1	5×10^{16}	30×30
P2	5×10^{15}	30×30

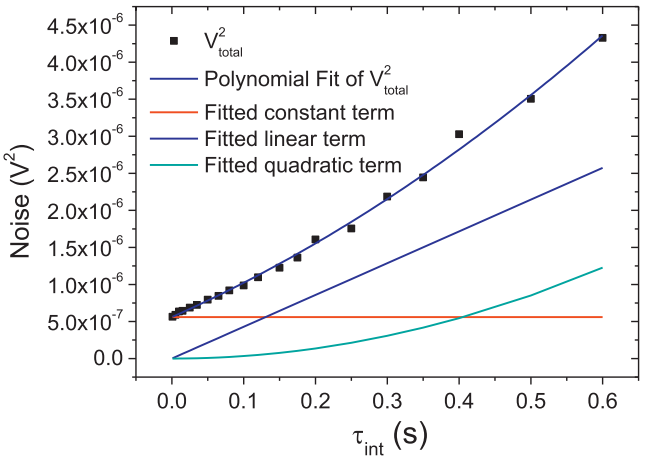

Fig. 4. The $V^2_{total} - \tau_{int}$ curve of S1 at room temperature and its polynomial fitting curve.

overtake the constant until the integration time gets to 0.12 s, and after that the linear noise would be much more important than the constant. This agrees with the analysis mentioned above.

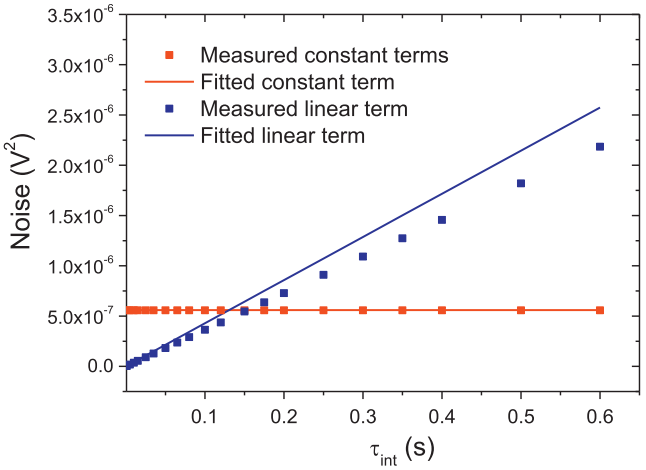

Fig. 6. The measured and fitted noise of S1 at room temperature.

The log V_{total} – log τ_{int} results of S1 and S2 and corresponding linear-fitting curves with their fitting slopes were shown in Fig. 7.

The slope of S1 is close to 0 when the integration time is below 0.02 s, but is close to 0.5 when the integration time is longer than 0.02 s. The slope of S2 is close to 0 with shorter integration time, too. However, with the increasing of integration time the slope of S2 increases to 1 rapidly. Obviously there is a turning point of slope change around integration time 0.1 s for S1, and for S2 this value drops to about 0.06 s. The results indicate that the coupled noise is dominant in noise characteristics for both S1 and S2 sample during shorter integration time. During the longer integration time,

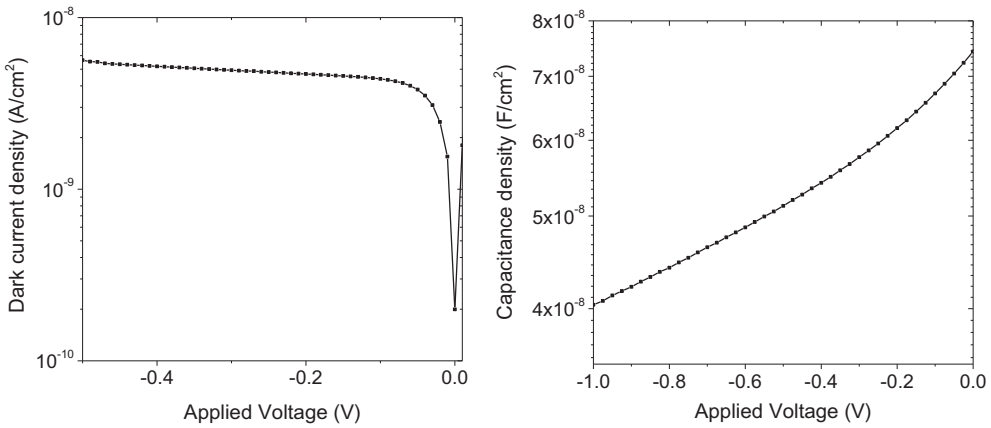

Fig. 5. I-V and C-V characteristic of S1 at room temperature.

the main source of S1 transfer to shot noise, while for sample S2 the ROIC fixed pattern noise and detectors flicker noise have more effect due to the negligible shot noise.

The noise of S2 is lower than S1 in shorter integration time when coupled noise is the major contributor to FPAs noise, which indicates the detector capacitance of S2 is lower than S1. The detector capacitance of sample S2 calculated from coupled noise is about one-third of S1. The capacitance density of p^+n junction can be represented by [17],

$$C_d = \left[\frac{q\tau N_0}{2(V_{bi} - V)}\right]^{1/2}, \tag{9}$$

where τ is the minority carrier lifetime, N_0 is the doping concentration of absorption layer, V_{bi} is the built-in voltage. According to the relationship between C_d and applied voltage, N_0 can be calculated by linear fitting $\frac{1}{C_d^2} \sim V$, the fitting slope is $-\frac{2}{q\tau N_0}$. The $\frac{1}{C_d^2} \sim V$ curve and its linear fitting curve of S1 are shown in Fig. 8, the fitted slope is -3.06×10^{14}, so the fitted concentration of absorption layer is $3.3 \times 10^{16}\ \mathrm{cm}^{-3}$. According to the analysis of the relationship between C_d and N_0, the concentration in the absorption layer of S2 is approximately 10 times lower than that in S1.

As mentioned above, if detector capacitance decreases, the contribution of dark current will increases, which causes the increase of the slope of $\log V_{total} - \log \tau_{int}$ curves. The slope of S2 with shorter integration time is smaller than S1, and the coupled noise of S2 is lower than S1. As a result, the dark current of S2 is lower than S1. As shown in Fig. 9. The dark current of S2 was obtained by linear fitting the $V_{ds} - \tau_{int}$. The dark current of S2 is 2.46×10^{-14} A, lower than S1, which is consistent with the analysis above.

When integration time increases, the main source of S2 becomes ROIC fixed pattern noise and detector flicker noise. The same ROIC was adopted in S1 and S2, but the quadratic term doesn't impact the noise characteristic of S1. So the contributor of S2 during longer integration time should be detector flicker noise.

C-V and I-V characteristics of two kinds of photodiodes marked as P1 and P2 with different N_0 at room temperature were shown in Fig. 10. The detector capacitance of P1 with higher concentration of the absorption layer is 670 fF. The dark current of P1 is 3.96×10^{-14} A at 100 mV reverse bias and room temperature. The detector capacitance of P2 with lower concentration of absorption layer is 279 fF, lower than P1. The dark current of P2 is 4.02×10^{-13} A, about 10 times higher than P1. That is, to achieve

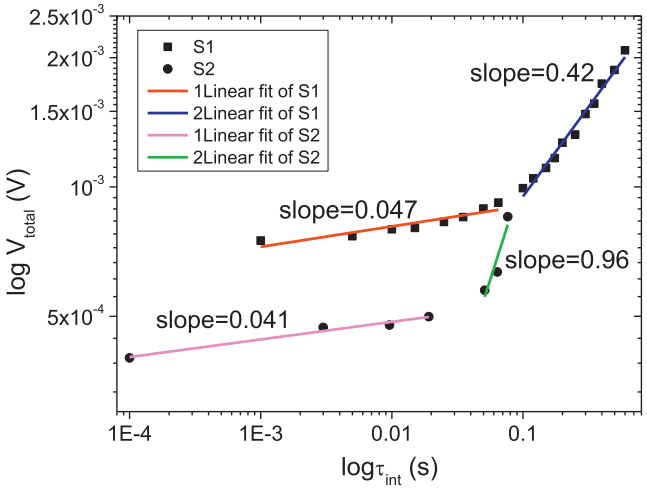

Fig. 7. The $\log V_{total} - \log \tau_{int}$ curves of InGaAs FPA marked by S1 and S2.

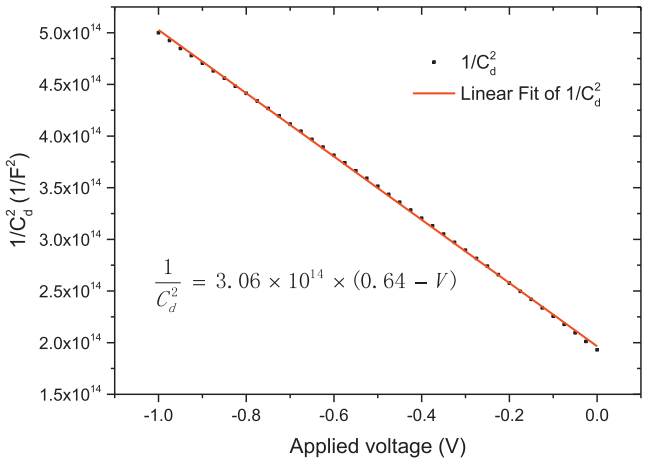

Fig. 8. The $\frac{1}{C_d^2} \sim V$ curve and its linear fitting curve of S1.

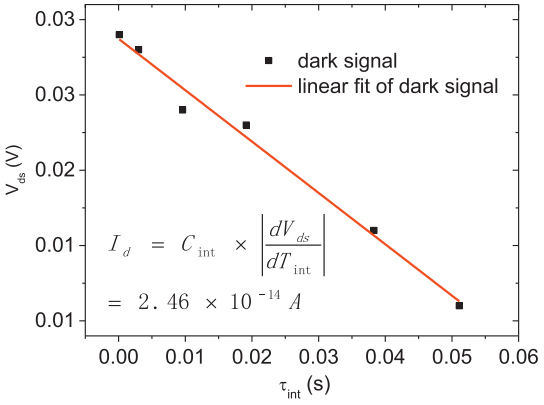

Fig. 9. The V_{ds}-τ_{int} curve and its linear fit curve of S2.

a lower detector capacitance level by decreasing N_0, the dark current has to largely rise up. There is a tradeoff between dark current and capacitance in detector chip design.

The $\frac{1}{C_d^2} \sim V$ curves and corresponding linear fitting curves of P1 and P2 are shown in Fig. 11. For P1, the fitted concentration of absorption layer is $2.4 \times 10^{16}\ \mathrm{cm}^{-3}$, close to the designed concentration $5 \times 10^{16}\ \mathrm{cm}^{-3}$. For P2, the fitted concentration is $4.28 \times 10^{15}\ \mathrm{cm}^{-3}$, very close to the designed concentration $5 \times 10^{15}\ \mathrm{cm}^{-3}$. The difference between calculated results and designed results may be caused by the errors in material growth progress or parasitic capacitance. Even so, the effects to reduce the capacitance of lowering N_0 is obvious.

The theoretical $\log V_{total} - \log \tau_{int}$ curves and corresponding linear fit curves with their fitting slopes were shown in Fig. 12. The noise of P2 is lower than P1 during the shorter integration time, and they are equal to each other when the integration time is 20 ms, then the noise of P2 is greater than P1 during the longer integration time. The lower noise performance of P1 with short integration time benefits from the decrease of detector capacitance. However, the noise of P2 increases rapidly with the increase of integration time as a result of higher dark current. Therefore, the challenge is to reduce the dark current of detectors with lower capacitance.

The influence of temperature on detector performance and FPAs total noise was studied. Fig. 13 demonstrates the curves of dark current density and detector capacitance to temperature for P1 and P2. It is obvious that the dark current density exponentially

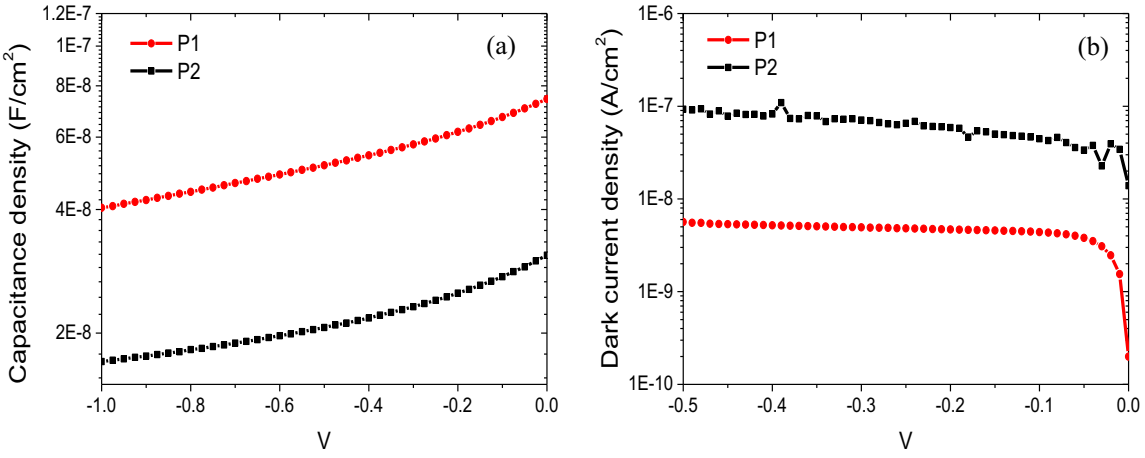

Fig. 10. C-V and I-V curves of two samples with different N_0. (a) C-V characteristic, (b) I-V characteristic.

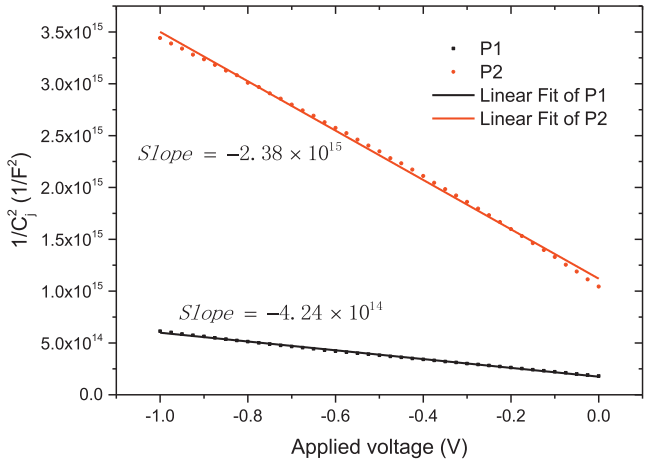

Fig. 11. The $\frac{1}{C_d^2} \sim V$ curves and corresponding linear fitting curves of P1 and P2.

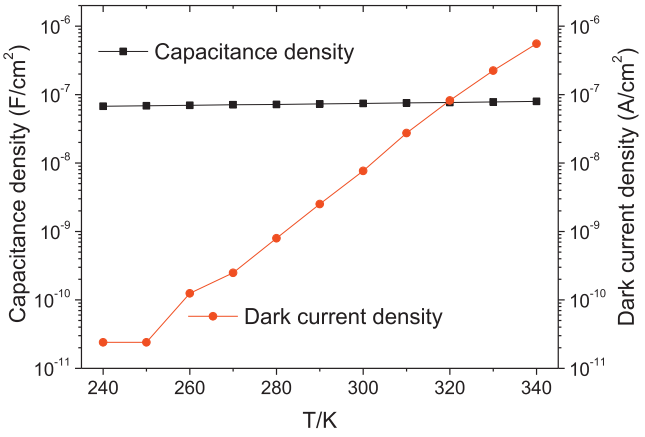

Fig. 13. Dark current and detector capacitance to temperature.

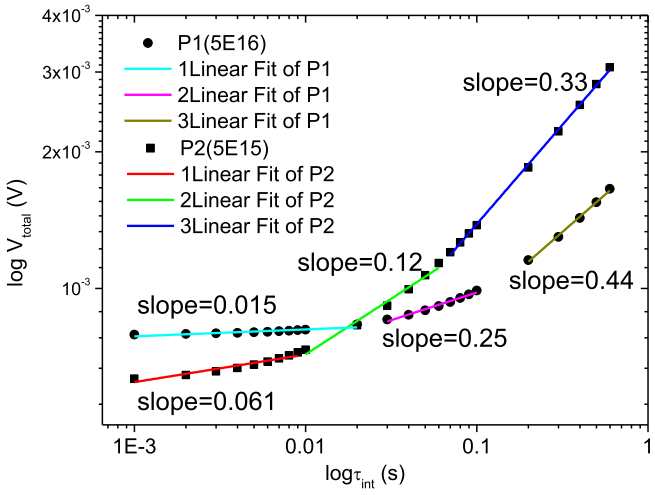

Fig. 12. The log V_{total} – log τ_{int} curves of InGaAs FPA marked by P1 and P2.

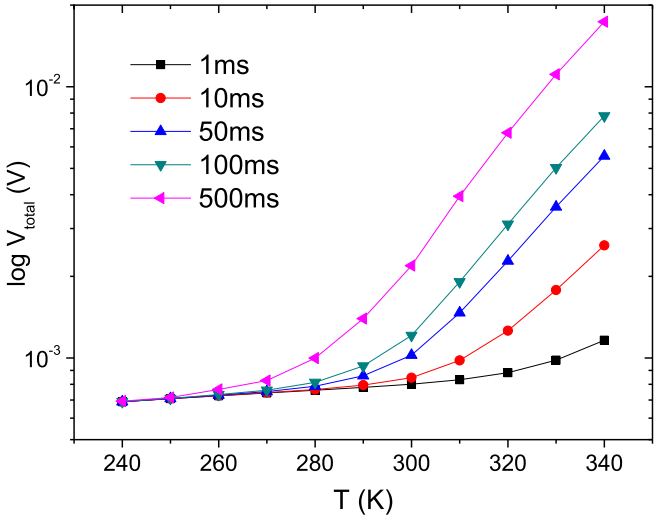

Fig. 14. The changing curves of noise with temperature.

with temperature decreasing. By contrast, the capacitance density is less dependent on the temperature.

The changing curves of P1's noise with the temperature in different integration time are shown in Fig. 14. When the temperature is very low, FPAs noise is nearly invariable with the integration time, because the dark current is so small that the detector capacitance becomes to the major contributor to FPAs noise. The noise of P1 decreases evidently with temperature especially during the longer integration time when dark current is

dominant. The effect of lowering temperature on reducing FPAs noise is mainly shown in the reduction of dark current.

5. Conclusions

The total noise in FPAs was analyzed mathematically. The influence factors of detector array performance on FPA noise such as dark current and detector capacitance were studied. For lower dark current level detectors, the effect of detector capacitance on noise is more remarkable. There is a pressing requirement of reducing the detector capacitance in order to achieve ultra-low noise FPAs especially in the shorter integration time, larger integration capacitance, and smaller pixel pitch. InGaAs FPA noise characteristics and detector performance were measured and analyzed. The calculated results can be well fitted to the measured data. When integration time is shorter, the influence of detector capacitance on noise is more dramatic than dark current. With the increasing of integration time, the contribution of dark current is increasing. The detector performance and its influence on FPAs noise in different conditions were measured and discussed. Decreasing N_0 was observed to show the opposite effect on dark current and capacitance. The reduction of detector capacitance results in the lowering of noise during shorter integration time, however the increase of dark current leads to the increase of noise during longer integration time. Lowering temperature is effective in lowering FPAs noise especially when the dark current is dominant in FPAs noise during longer integration time, because of the evident reduction of dark current.

Conflict of interest

The authors declared that they have no conflicts of interest to this work. We declare that we do not have any commercial or associative interest that represents a conflict of interest in connection with the work submitted.

Acknowledgements

Authors would like to acknowledge Prof. Zhang Yonggang from Shanghai Institute of Micro-system and Information Technology for the support for InGaAs material presented in this paper. The project is supported by National Natural Science Foundation of China (No. 61475179).

References

[1] Xue Li, Haimei Gong, Jiaxiong Fang, et al., The development of InGaAs short wavelength infrared focal plane arrays with high performance, Infrared Phys. Technol. 80 (2017) 112–119, http://dx.doi.org/10.1016/j.infrared. 2016.08.012.
[2] Xu. Jiao, Xiaoshuang Chen, Wenjuan Wang, Lu. Wei, Extracting dark current components and characteristics parameters for InGaAs/InP avalanche photodiodes, Infrared Phys. Technol. 76 (2016) 468–473.
[3] Y. Arslan, F. Oguz, C. Besikci, Extended wavelength SWIR InGaAs focal plane array: characteristics and limitations, Infrared Phys. Technol. 70 (2015) 134–137.
[4] X.D. Wang, W.D. Hu, X.S. Chen, W. Lu, H.J. Tang, T. Li, H.M. Gong, Dark current simulation of InP/$In_{0.53}Ga_{0.47}As$/InP p-i-n photodiode, Opt. Quant. Electron. 40 (2008) 1261–1266.
[5] M. MacDougal et al., Short-wavelength infrared imaging using low dark current InGaAs detector arrays and vertical-cavity surface-emitting laser illuminators, Opt. Eng. 50 (2011) 061011.
[6] A. Rogalski et al., Recent progress in infrared detector technologies, Infrared Phys. Technol. 54 (3) (2011) 136–154.
[7] K. Peter Judd, Jonathan M. Nichols, J. Grant Howard, et al., Passive shortwave infrared broadband and hyperspectral imaging in a maritime environment, Opt. Eng. 51 (1) (2012), 013202-1-013202-13.
[8] B.F. Andresen et al., Low dark current small pixel large format InGaAs 2D photodetector array development at Teledyne Judson Technologies, SPIE 8353 (2012), 835309-1-835309-8.
[9] Andrew D. Hood et al., Large-format InGaAs focal plane arrays for SWIR imaging, SPIE 8353 (2012).
[10] Atul Joshi, John Stevens, Anzhelika Kononenko, John Blackwell, Ultra-low noise high frame rate ROIC for visible and infrared focal plane arrays, SPIE 5499 (2004) 228–239.
[11] Ping Yuan, James Chang, Joseph C. Boisvert, et al., Low-dark current 1024×1280 InGaAs PIN arrays, SPIE 9070 (2014) 907007-1–907007-6.
[12] D. Mark et al., Nelson general noise processes in hybrid infrared focal plane arrays, Opt. Eng. 30 (No. 11) (1991).
[13] Huang Zhangcheng et al., Design of 800×2 low-noise readout circuit for near-infrared InGaAs focal plane array, SPIE 8562 (2012) 856205-1–856205-7.
[14] Eric de Borniol et al., High-performance 640 × 512 pixel hybrid InGaAs image sensor for night vision, SPIE 8353 (2012), 835307-1- 835307-8.
[15] Jerris F. Johnson et al., Focal-plane signal and noise model–CTIA ROIC, IEEE Trans. Electron Devices 56 (11) (2011) 2506–2515.
[16] Xue Li, Yu. Songlei Huang, Hengjing Tang Chen, Xiumei Shao, et al., Noise characteristics of short wavelength infrared InGaAs linear focal plane arrays, J. Appl. Phys. 112 (2012) 064509.
[17] Donald A. Neamen, Semiconductor Physics and Devices, Chapter 7, Publishing House of Electronics Industry, 2011: 241-267